



This is the accepted manuscript made available via CHORUS. The article has been published as:

Soft-phonon anomalies and crystal electric field-phonon coupling in cubic lanthanide sesquioxides Eu_2O_3 and Yb_2O_3

J. E. Slimak, A. Cote, G. J. MacDougall, and S. L. Cooper

Phys. Rev. B **108**, 045128 — Published 17 July 2023

DOI: [10.1103/PhysRevB.108.045128](https://doi.org/10.1103/PhysRevB.108.045128)

Soft Phonon Anomalies and Crystal Electric Field-Phonon Coupling in Cubic Lanthanide Sesquioxides: Temperature-dependent and Magneto-Raman Scattering Studies of Eu_2O_3 and Yb_2O_3

J. E. Slimak, A. Cote, G. J. MacDougall, and S. L. Cooper

*Department of Physics and Materials Research Laboratory,
University of Illinois, Urbana, Illinois 61801, USA*

(Dated: May 11, 2023)

Phonon softening is a common identifier of strong coupling between electronic and vibrational degrees of freedom in materials, which is responsible for many of the exotic phenomena observed in scientifically interesting and technologically relevant materials. Two cubic rare earth sesquioxides (RESO), Eu_2O_3 and Yb_2O_3 , display anomalously soft phonons compared to trends in phonon energy exhibited by other cubic RESOs. In an effort to elucidate the mechanisms responsible for the anomalous mode softening in Eu_2O_3 and Yb_2O_3 , we performed temperature- and magnetic field-dependent Raman scattering studies of polycrystalline samples of these materials. Our data suggest that two different underlying phenomena are responsible for these anomalies. While we observe crystal electric field (CEF) electronic transitions in both materials, only in Yb_2O_3 does the energetic proximity of CEF excitations to phonons appear to lead to significant electron-phonon coupling in the form of CEF-phonon coupling. We find evidence that defects—rather than interactions between vibrational and electronic excitations—are responsible for the soft phonons in Eu_2O_3 . These results place constraints on proposed phonon mode softening mechanisms in rare-earth sesquioxides and illustrate the varied effects of electron-phonon coupling in these materials.

I. Introduction

Strong electronic coupling to lattice degrees of freedom in crystals is one of the most important mechanisms by which scientifically interesting and technologically important materials properties arise. Clarifying the interactions between phonons and electrons is critical to understanding the mechanisms responsible for a variety of exotic phenomena in materials—including cooperative and dynamical Jahn-Teller effects [1–4], giant magnetocapacitance [5, 6], and multiferroicity [7]—and to developing new functional materials to control future devices [8].

The rare earth sesquioxides (RESO) are a class of chemically simple materials that are nevertheless excellent laboratories for observing the complex interactions between electronic and lattice degrees of freedom [5, 6, 9, 10]. Because the $4f$ -orbital states of the lanthanide sesquioxides are spatially localized on the ionic nuclei, these states are only weakly split by the surrounding crystal field environment. Weak crystal field splitting leads to low-lying electronic excitations that are close in energy to lattice vibrations, providing an opportunity for significant interaction and/or hybridization between electronic and phonon excitations. In the presence of a sufficiently strong interaction, as in CeAl_2 [11, 12], CeCuAl_3 [13], Ce_2O_3 [6], TbInO_3 [14], or $\text{Ho}_2\text{Ti}_2\text{O}_7$ [15], the degree of mixing between phonon and electronic excitations can lead to new excitations with significant mixed character, known as vibronic excitations.

Many materials having strong electron-phonon coupling exhibit anomalies in their vibrational spectra. For example, the phonon energies in most cubic rare earth sesquioxides (RESOs) vary linearly with the lattice parameter [23], as shown in Figure 1. However, the energies of many Raman-active phonons in Eu_2O_3 and Yb_2O_3 de-

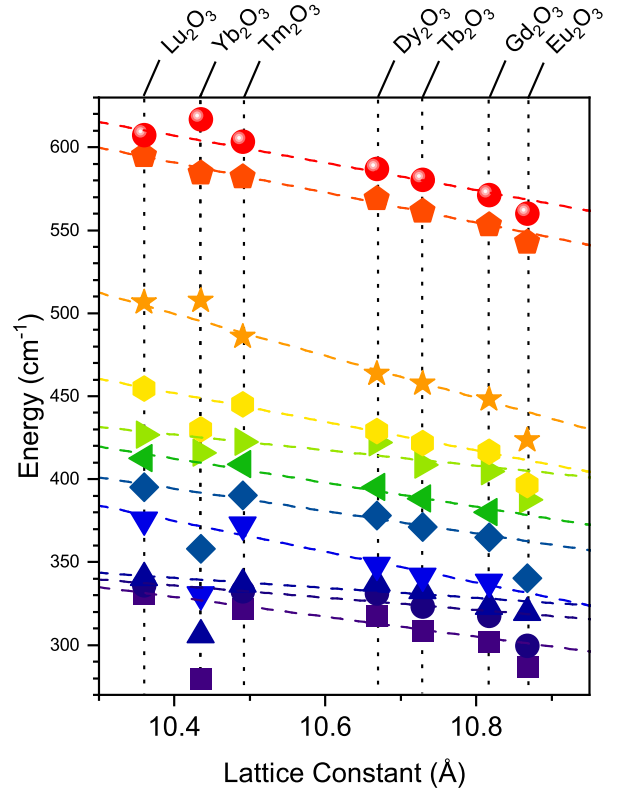


FIG. 1. Summary plot of the energies of the Raman-active phonons for various C-type RESOs as measured by the authors at $T = 3$ K, as functions of the lattice constant of the RESO. Trendlines are linear fits of the data, omitting Yb_2O_3 and Eu_2O_3 , to highlight the anomalous behavior of the two materials. Lattice constant data from Refs [16–22].

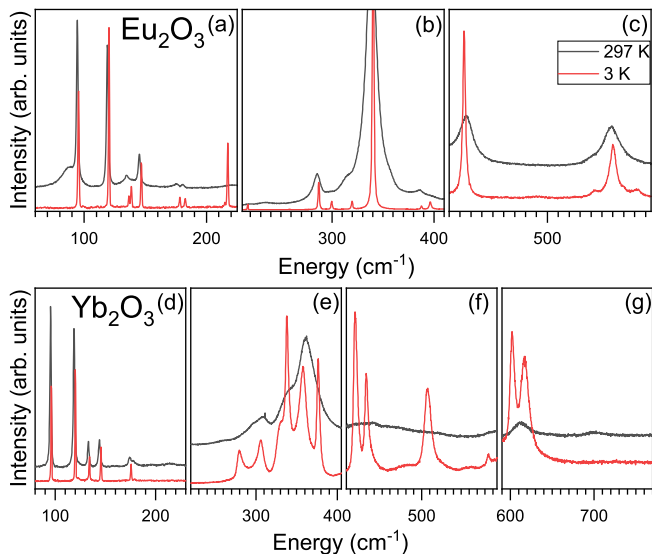


FIG. 2. Raman spectra of (a – c) Eu_2O_3 and (d – g) Yb_2O_3 at room temperature (black) and 3 K (red). Individual spectra have been offset vertically for clarity.

viate from these trends [23–25]. Specifically, the phonons having energies between 250 cm^{-1} and 510 cm^{-1} in Eu_2O_3 and Yb_2O_3 are significantly softer than predicted by the trend exhibited by other RESOs [23–25], while the highest energy phonon in Yb_2O_3 has a markedly higher energy than would be expected by the trend. Previous reports of the Raman and IR spectra of Eu_2O_3 and Yb_2O_3 by Urban and Cornilsen suggest that the anomalous phonon energies in these materials result from weaker chemical bonding and shallower interatomic potentials [25]. By contrast, Schaack and Koningstein propose that low energy crystal field excitations couple to the phonons, leading to the anomalous phonon behavior [24]. Yet another explanation for these phonon anomalies has been proposed more recently, particularly in the case of Eu_2O_3 , wherein oxygen vacancy defects are attributed to the soft phonon behaviors [23]. However, Eu_2O_3 lattice dynamical calculations provide evidence that disputes this hypothesis [26].

Raman scattering studies of rare-earth sesquioxides offer a powerful method for elucidating the origins of CEF-phonon coupling in these materials, generally, and for testing the theories of phonon anomalies in Eu_2O_3 and Yb_2O_3 , more specifically. In this paper, we report a study of electron-phonon coupling effects in Eu_2O_3 and Yb_2O_3 , focusing on CEF-phonon coupling effects, using temperature-dependent (3 – 300 K) and magnetic-field-dependent (0 – 7 T) Raman scattering experiments. We can clearly discern, for the first time to our knowledge, the positions of all the strong Raman-active phonons and confirm the energies of many of the low-lying crystal electric field (CEF) electronic excitations in Eu_2O_3 and Yb_2O_3 . Our measurements reveal evidence of defect-induced behavior in Eu_2O_3 , which may explain the

anomalous phonon softening in this material. We find evidence that CEF-phonon coupling in these materials is important for understanding anomalous temperature-dependences of phonons having energies between $250 - 650\text{ cm}^{-1}$ in both Eu_2O_3 and Yb_2O_3 . However, our results suggest that CEF-phonon coupling in Eu_2O_3 is weaker than in Yb_2O_3 and largely arises because of lattice vacancy defects which have been reported to occur in Eu_2O_3 crystals [27–29]. While, we do not find evidence for defects in the spectra of Yb_2O_3 , we do observe that Yb_2O_3 exhibits significant anomalies in phonon energies, intensities, and linewidths as functions of temperature and magnetic field, indicative of strong coupling between phonons and low-lying CEF electronic excitations in this material.

II. Experimental

Polycrystalline samples of cubic Eu_2O_3 and Yb_2O_3 were prepared from commercially available powders (Alfa Aesar) with 99.996% and 99.99% purities, respectively. Disks of pressed powder were sintered in a box furnace under ambient atmosphere at $1000\text{ }^\circ\text{C}$ for 36 hours before being fractured into small fragments. This high temperature treatment is necessary to eliminate contamination from rare earth carbonates, hydrates, and hydroxides formed by reactions between the oxides and carbon dioxide and water in the atmosphere. Sample fragments were stored under positive nitrogen pressure in a desiccator box to minimize contamination.

Inelastic light (Raman) scattering measurements were performed using the 647.1 nm excitation of a Coherent Innova 70C Kr^+ laser. The scattered light was collected in a backscattering geometry by dispersing through a custom triple-grating spectrometer and recorded with a liquid nitrogen-cooled charge-coupled-device detector. Samples were held in a continuous He-flow cryostat and horizontally mounted in the open bore of a superconducting magnet. This experimental arrangement allows Raman scattering measurements to be conducted under simultaneous control of the temperature (3 – 300 K) and magnetic field (0 – 7 T). Spectra obtained were in the energy range of approximately $20 - 955\text{ cm}^{-1}$. All magnetic field-dependent measurements were performed in the Faraday geometry with the incident light wave vector parallel to the magnetic field. The incident light was circularly polarized, and scattered light of all polarizations was collected.

III. Results and Discussion

The RESOs comprised of rare earth constituents heavier than Sm crystallize in the cubic, C-type structure with space group $Ia\bar{3}$ [24]. The unit cell of this structure features two types of symmetry inequivalent rare earth ion sites, occupying the $8b$ and $24d$ Wyckoff positions, with C_2 and S_6 symmetries, respectively, and oxygen ions in the $48e$ sites [24]. The twenty-two zone-center, Raman-active phonons for this structure are given by $\Gamma_{\text{Raman}} = 14A_g + 4E_g + 4T_g$. However, previous Ra-

TABLE I. Energies of Raman-active Phonons in Eu_2O_3 and Yb_2O_3 in cm^{-1} and their irreducible representations (IR). The symmetry of each phonon in this table is given by the associated irreducible representation (IR) of the space group $Ia\bar{3}$ in the right-most column. The second and fifth columns are the results of this study. For results published by other authors, the symmetry analyses of their results have not been altered in this table, despite disagreements between the results of density functional theory (DFT) and Raman studies.

Eu_2O_3 Energy from DFT ^a	Eu_2O_3 Energy from Raman	Eu_2O_3 Energy from Raman ^b	Eu_2O_3 Energy from Raman ^c	Yb_2O_3 Energy from Raman	Yb_2O_3 Energy from Raman ^d	IR ^a
92.634	95.2	—	94	96.1	99.2	T_g
97.116	—	—	109	102	—	T_g
115.535	120.2	—	119	120	121	A_g
130.337	136.4	—	134	134.3	—	T_g
140.698	146.6	—	145	145.5	—	E_g
168.224	178.148	—	—	175.5	—	T_g
173.005	182.6	—	175	179.2	—	T_g
277.061	—	—	—	—	—	T_g
285.673	287.3	266.4	289	279.7	279	T_g
292.68	299.7	—	—	306.5	305	E_g
304.218	—	—	—	—	—	T_g
313.276	319.6	—	—	331.2	—	A_g
327.793	—	—	—	—	—	T_g
330.202	—	—	—	—	—	E_g
348.414	340.4	336	339	357.6	358	T_g
373.941	387.8	—	385	415.5	420	A_g
381.566	396.3	380	—	430.3	443	T_g
407.908	423.5	—	425	507	—	T_g
477.2	—	459	—	—	—	T_g
513.872	543	—	—	584	—	A_g
520.226	560	—	—	602	—	E_g
535.489	569	—	559	618	621	T_g

^a Results from Ref. [26]

^b Results from Ref. [30]

^c Results from Ref. [23]

^d Results from Ref. [24].

man spectroscopic studies of both Eu_2O_3 and Yb_2O_3 have observed only some of the Raman-allowed phonons [23, 24, 30–32]. Figure 2 presents our Raman scattering spectra of both (a – c) Eu_2O_3 and (d – f) Yb_2O_3 obtained at 297 K (upper, black curves) and 3 K (lower, red curves). We observe several phonons in the Yb_2O_3 and Eu_2O_3 spectra that have not been previously reported. Because we measured polycrystalline samples, we were unable to perform the polarization-dependent studies necessary to completely determine the symmetries of the phonons. However, previous studies of single-crystal C-type RESOs [24] and lattice dynamical calculations performed by Łażewski et al. [26] allow us to tentatively assign symmetries to all the observed phonons. We present these assignments in Table I, alongside comparisons to previous Raman scattering studies of Eu_2O_3 and Yb_2O_3 . Future studies of these materials would greatly benefit from single crystals, allowing more clear determination of the symmetries of the excitations.

In the spectra obtained at 3 K, we observe several additional features that are consistent with electronic transitions between CEF-split electronic states of the rare earth ions in both Eu_2O_3 and Yb_2O_3 . These features are energetically consistent the measured energies of transitions observed in luminescence experiments in Eu_2O_3

and with the energies of CEF levels obtained from fitting Schottky anomalies in Yb_2O_3 heat capacity data [33]. Additionally, we are able to rule out that these features are spin-wave excitations, because there is no long-range magnetic order in these materials. Eu_2O_3 and Yb_2O_3 exist in their paramagnetic phases over the entire ranges of temperature, pressure, and magnetic field explored in these experiments [34, 35]. We are also able to rule out that these are additional phonon modes on the basis that there is no experimental or theoretical evidence for temperature-dependent structural transitions in either Eu_2O_3 or Yb_2O_3 between $T = 3 - 300$ K. Finally, the dramatic temperature-dependent increase in spectral weight with decreasing temperature of these features is consistent with their electronic origin, owing to increasing population of the initial state (the ground state) associated with the transitions.

The energies of the observed CEF transitions are summarized in Table II, along with the expected symmetries of the excited states in cases where the symmetry of the state can be confidently determined and results from previous experiments and calculations [10, 33]. In the following, we present the spectroscopic features observed in (III A) Eu_2O_3 and (III B) Yb_2O_3 , we summarize the dependences of these spectroscopic features on temperature

TABLE II. Energies of Low Energy CEF Excitations in Eu_2O_3 and Yb_2O_3 in cm^{-1} . The results in the second and fourth columns are from this study.

Eu_2O_3 Energy from Lumines- cence ^a	Eu_2O_3 Energy from Raman	Yb_2O_3 Energy from Raman ^b	Yb_2O_3 Energy from Raman	R^{3+} Ion Site Symmetry
139	139			S_6
217	217			C_2
		334	336	C_2
351	—			C_2
		388	376	S_6
423	—			S_6
537	—			C_2
		595	601	C_2
		740	—	S_6
		980	—	S_6
		1021	—	C_2

^a Results from Ref. [10].

^b Results from Ref. [33].

and applied magnetic field, and we discuss what these results reveal concerning the significant roles of strong CEF-phonon coupling in these materials.

A. Eu_2O_3

1. Phonons at 3 K

Our results on Eu_2O_3 presented in Figure 2 (a – c) reveal narrow phonons in the 3 K spectra, consistent with published spectra of other C-type RESOs [23, 24], and our own unpublished results on RESOs. Of the twenty-two Raman-allowed phonons in Eu_2O_3 , we observe seventeen phonons in Eu_2O_3 , several more than have been previously reported. The phonon energies we measure agree well with the energies predicted using density functional theory calculations up to an energy of approximately 340 cm^{-1} [26]. For observed phonons in Eu_2O_3 having energies higher than 340 cm^{-1} , the predicted energies underestimate our measured energies by up to 35 cm^{-1} .

2. CEF Excitations

The ground state of a free Eu^{3+} ion is unique amongst the RE ions in that it is singlet state, with term symbol 7F_0 . Additionally, the first excited level is much closer in energy to the ground state than in many RE ions, being separated by only approximately 300 cm^{-1} ($\approx 40 \text{ meV}$). The relatively low first-excited state CEF energy holds true for the Eu^{3+} ions in Eu_2O_3 as well, based on our Raman scattering results and earlier luminescence spectroscopy results [10]. Given the site symmetries of the Eu^{3+} ions in Eu_2O_3 , the states and symmetries of the excited 7F_1 manifolds of the two types of symmetry inequivalent RE ions can be determined without knowing the associated energy levels. In C_2 symmetry, the degeneracy of the 7F_1 manifold is fully lifted by the CEF, yielding one state with A symmetry given by $|J_z = 0\rangle$,

and two states with B symmetry that are given by linear combinations of the J_z eigenstates $|J_z = +1\rangle \pm |J_z = -1\rangle$. In S_6 symmetry, the degeneracy of the 7F_1 manifold is only partially lifted, resulting in two levels—one with A_u symmetry, given by the state $|J_z = 0\rangle$, and the other with E_u symmetry, comprised of the degenerate J_z eigenstates $|J_z = +1\rangle$ and $|J_z = -1\rangle$.

In our Raman spectra of Eu_2O_3 , we expect to observe three transitions from the ground state to the excited 7F_1 levels of the C_2 Eu^{3+} ions, given that all these transitions are Raman-allowed. Transitions from the ground state to the excited levels of the 7F_1 manifold of the S_6 Eu^{3+} ions are parity forbidden, given that these states occur with ungerade symmetry, and are therefore Raman-forbidden. Unexpectedly, our results presented in Figure 3 show that we observe two resonances having energies and temperature dependences consistent with transitions between the ground and excited CEF states [10]. We can confidently assign the 217 cm^{-1} excitation to the CEF electronic transition from the ground state to the first excited CEF level of the C_2 Eu^{3+} ions, based on analyses of the lumi-

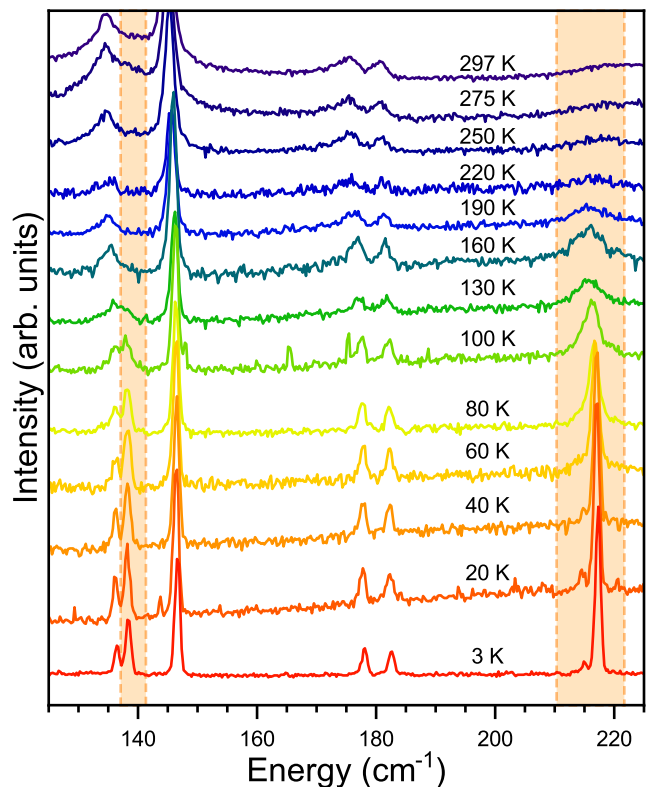


FIG. 3. Temperature dependence of the two observed CEF excitations in Eu_2O_3 with energies at $T = 3 \text{ K}$ of 138.4 and 217.3 cm^{-1} . The CEF excitations are in the regions shaded in orange. There is a phonon at 136.4 cm^{-1} which is nearly coincident with one CEF excitation. Additionally, there is a weak sideband to the 217.3 cm^{-1} CEF excitation at 214.9 cm^{-1} with similar temperature dependence, suggesting that it is a related feature. Individual spectra have been offset vertically for clarity.

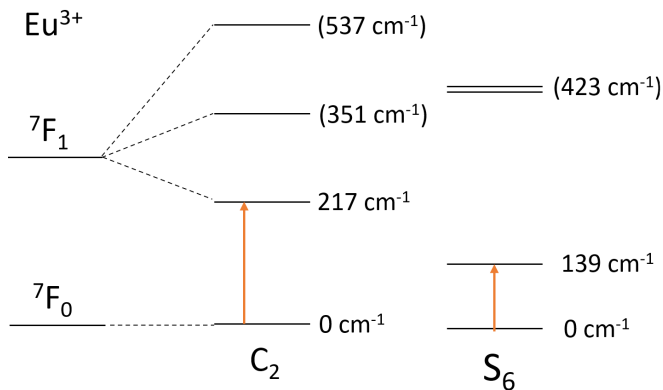


FIG. 4. Proposed low energy CEF level schemes for both Eu^{3+} ion sites in Eu_2O_3 . Arrows depict the observed transitions from the ground state to excited states. Energies presented in parentheses are of levels not observed in this study, but instead are obtained from Ref [10].

nescence intensity ratios by Buijs, et al. [10]. Further, we tentatively assign the 139 cm^{-1} excitation to the Raman-forbidden electronic transition from the ground state to the first excited CEF level of the S_6 ions (see Figure 4), based on the same analysis as previously mentioned [10]. There is no evidence in the spectra obtained at 3 K for any higher energy CEF transitions associated with either the C_2 or S_6 sites. Based on these measurements, we propose a level diagram, shown in Figure 4, for the CEF splitting of the 7F_1 manifold of the C_2 and S_6 symmetry ions in Eu_2O_3 . The energies of these CEF excitations and the Eu^{3+} ion site they are associated with are summarized in Table II.

The anomalous presence of the Raman-forbidden 139 cm^{-1} CEF transition suggests either a breakdown of the Raman selection rules in this system, or that the Eu^{3+} ions previously reported to occupy the S_6 site instead occupy a lattice site with lower symmetry. Beyond the two clear CEF transitions, we also observe a small secondary feature in our Raman spectra of Eu_2O_3 , shown in Figure 3, having an energy of approximately 214 cm^{-1} at 3 K. The presence of this additional peak suggests that some of the C_2 site Eu^{3+} ions experience a different CEF environment, leading to a lower energy first excited level. We propose that structural defects prevalent in crystals of Eu_2O_3 [27–29] are the likely origin of the breakdown of Raman selection rules, specifically regarding the 139 cm^{-1} parity-forbidden transition associated with the S_6 site and the presence of the additional 214 cm^{-1} transition. We discuss the substantial evidence for the presence of defects through their dramatic impact on the spectra of Eu_2O_3 in the following subsection.

3. Temperature-dependent Anomalies

Our temperature-dependent Raman scattering measurements of Eu_2O_3 reveal anomalous softening of the

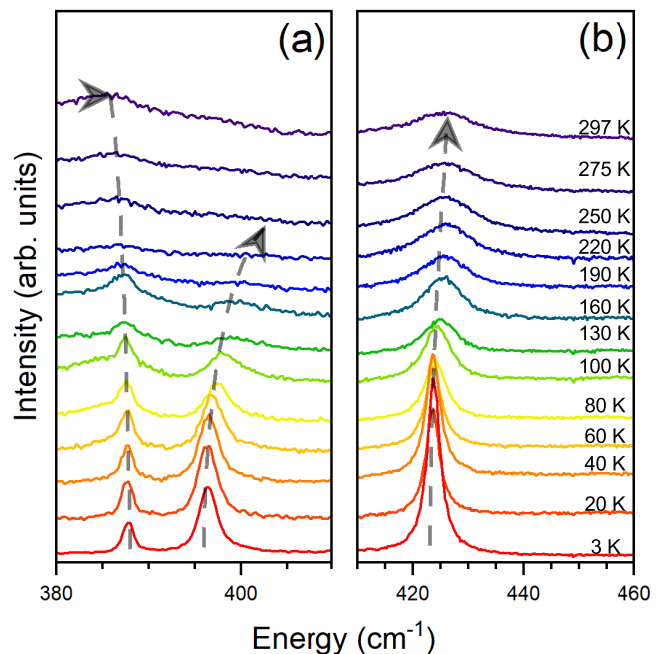


FIG. 5. Temperature dependence of the soft phonons in Eu_2O_3 with energies at $T = 3\text{ K}$ of (a) 396.4 and (b) 423.5 cm^{-1} . Arrows are included as guides to the eye, including an example of a phonon with normal temperature dependence having an energy at $T = 3\text{ K}$ of 387.8 cm^{-1} . Individual spectra have been offset vertically for clarity and the vertical scales are different between the subfigures.

396.4 and 423.5 cm^{-1} phonons with decreasing temperature, shown in Figure 5. Previous studies of Eu_2O_3 have identified a CEF excitation having an energy of 423 cm^{-1} [10]. We propose that a weak vibronic coupling exists between the 396.4 and 423.5 cm^{-1} phonons and this 423 cm^{-1} CEF excitation, leading to an avoided level repulsion between these coupled excitations. Given that shared symmetry is an essential component of vibronic coupling, and that the 7F_1 states of the S_6 ion have ungerade symmetry rather than the gerade symmetry associated with the Raman active phonons, vibronic coupling between these modes can occur only if there is a lowering of the symmetry of the S_6 site—specifically, a loss of inversion symmetry facilitated by structural defects.

In addition to the anomalous softening of the 396.4 and 423.5 cm^{-1} modes, we observe additional features in spectra obtained at temperatures near 300 K, shown in Figure 6. These features have broad linewidths and dramatically temperature-dependent intensities, losing intensity as the temperature is lowered and disappearing in spectra obtained below 200 K. Given this dramatic temperature dependence, we can rule out two-phonon excitations as an explanation of these features.

While the 87 and 134 cm^{-1} features are nearly energetically coincident with transitions originating from the first excited levels of the Eu^{3+} ions, we can largely rule

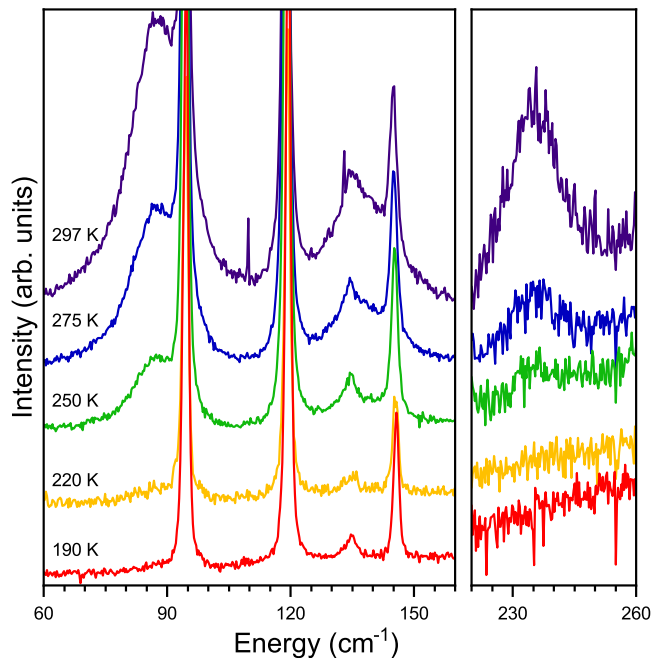


FIG. 6. Temperature dependences of the anomalous excitations present in the Eu_2O_3 spectra near room temperature. Individual spectra have been offset vertically for clarity and the vertical scales are different between the subfigures.

out that these features are transitions originating from thermally populated excited CEF levels. This explanation for the presence of these peaks fails to account for the 234 cm^{-1} feature, for which there is not an energetically coincident CEF transition between excited CEF levels. Additionally, if these features were transitions originating from excited states, we would expect to observe the 87 and 234 cm^{-1} peaks down to a lower temperature than the 134 cm^{-1} peak.

A more convincing interpretation of these features is suggested by luminescence measurements of Eu_2O_3 and Eu^{3+} -doped Y_2O_3 and Gd_2O_3 , where energy transfer reactions are observed [10]. In materials where the electronic excitations are localized by disorder, energy transfer reactions can occur, whereby the energy associated with an electronic excitation at one lattice site is transferred to another lattice site [10, 36]. In resonant cases, this can happen without mediation by phonons. However, if there is an energy mismatch between the excitations associated with the two lattice sites, phonons having the appropriate energy can mediate the transfer of energy from one lattice site to the other [10]. The energies of these strongly temperature-dependent features in our Raman spectra of Eu_2O_3 (87 , 134 , and 234 cm^{-1}) are well aligned with the energies reported to be involved in energy transfer reactions between 5D levels in Eu_2O_3 [10]. The energies of these features also closely match those calculated for three infrared-active phonons, which have the appropriate ungerade symmetries required to facilitate energy transfer from C_2 to S_6 symmetry Eu^{3+}

ions [26]. Further, the dramatic temperature dependence of these features is more consistent with the temperature dependence of energy transfer reactions observed in Eu^{3+} -doped Y_2O_3 and Gd_2O_3 , where the reaction rate goes as $R \sim T^7$ [10]. Consequently, we argue that in addition to the other defect-induced effects described above, the presence of defects in Eu_2O_3 facilitate energy-transfer coupling between the 5D_J electronic manifolds and infrared-active phonons of Eu_2O_3 leading to a breakdown in the Raman selection rules.

B. Yb_2O_3

1. Phonons at 3 K

We can confidently identify nineteen of the twenty-two Raman-active phonons in Yb_2O_3 based on our measurements performed at 3 K, presented in Figure 2 (d – g). As previously reported by Schaack and Koningstein [24], the phonons having energies greater than 250 cm^{-1} in our Yb_2O_3 spectra are broadened even at 3 K, while those having lower energies display narrow linewidths similar to those of the other C-type RESOs. This intrinsic broadening at low temperatures has been previously attributed to strong electron-phonon coupling—arising either from the energetic proximity of CEF levels to these phonons [24] or from modulation of the interatomic potential by shallow electronic levels below the Fermi level [25]. Indeed, we show in the following sections that Yb_2O_3 exhibits several CEF excitations that are nearly resonant with these phonons, and the energetic proximity of these CEF excitations to the phonons create favorable conditions for vibronic coupling between these degrees of freedom.

2. CEF Excitations

A free Yb^{3+} ion has an eightfold degeneracy associated with its ground state, given by the term symbol $^2F_{7/2}$. However, in a crystal, this degeneracy is lowered by the electrostatic potential produced by the ions surrounding a given Yb^{3+} ion, yielding a manifold of CEF levels that are only weakly split in energy. The ground states of both the $8b$ and $24d$ Yb^{3+} ions in Yb_2O_3 are split into manifolds of four doubly degenerate levels. These low-lying Yb_2O_3 CEF states are well approximated by admixtures of J_z eigenstates of the Yb^{3+} free ion $^2F_{7/2}$ manifold. In this approximation, the S_6 states take on one of two generalized forms: the first, shown in Eq. 1, has $A_{3/2g}$ symmetry; the second, shown in Eq. 2, has $E_{1/2g}$ symmetry. On the other hand, the C_2 states take on the form given by Eq. 3, which has $E_{1/2}$ symmetry. In Eqs. 1 – 3, the kets are labeled by their J_z eigenvalues and coefficients $A - I$ are factors determined by diagonalization of the CEF Hamiltonian associated with each site to yield appropriately normalized states:

$$A \left| +\frac{3}{2} \right\rangle + B \left| -\frac{3}{2} \right\rangle \quad (1)$$

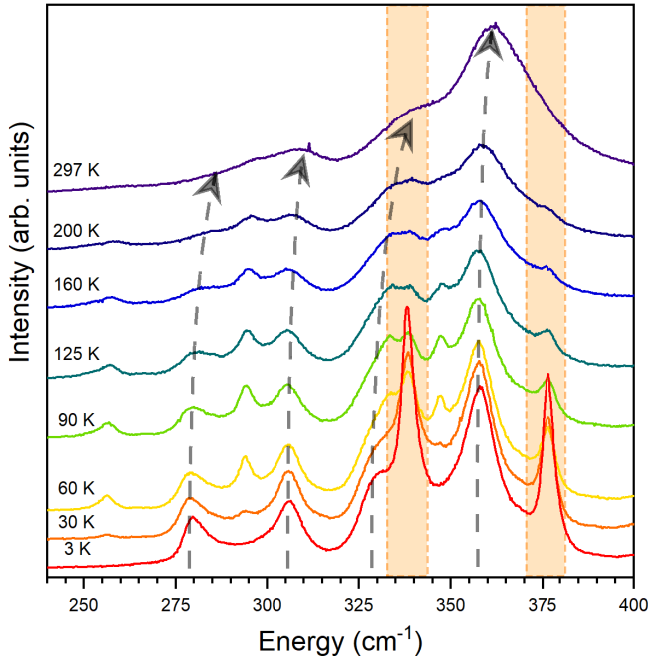


FIG. 7. Temperature dependence of the soft phonons in Yb_2O_3 with energies at $T = 3\text{K}$ of approximately 279.7, 306.5, 331.2 and 357.6 cm^{-1} and the two of the three observed CEF excitations with energies of approximately 338 and 378 cm^{-1} . Arrows are included as guides to the extent of the phonon softening with temperature. The crystal field excitations are highlighted in orange. Individual spectra have been offset vertically for clarity.

$$C \left| \pm \frac{7}{2} \right\rangle + D \left| \pm \frac{1}{2} \right\rangle + E \left| \mp \frac{5}{2} \right\rangle \quad (2)$$

$$F \left| \pm \frac{7}{2} \right\rangle + G \left| \pm \frac{3}{2} \right\rangle + H \left| \mp \frac{1}{2} \right\rangle + I \left| \mp \frac{5}{2} \right\rangle \quad (3)$$

Our Raman spectra of Yb_2O_3 reveal excitations having energies of 336, 376, and 601 cm^{-1} , presented in Figures 7 and 8, which we assign to CEF electronic excitations from the ground state to excited levels of the ${}^2F_{7/2}$ manifolds of both the C_2 and S_6 ions (see Figure 9). This assignment is consistent with previous analyses by Schaack and Koningstein [24] and Gruber et al. [33]. These CEF excitations are absent or nearly absent at room temperature and gain substantial intensity as the temperature is decreased, consistent with the expectation that CEF transitions from the ground state to these excited states gain intensity as the ground state CEF level becomes less thermally depopulated at low temperatures. Based on the analysis performed by Gruber et al. [33], we can confidently assign the 336 and 602 cm^{-1} excitations to electronic transitions from the ground state to the first and second excited levels of the C_2 symmetry ions, and we assign the 376 cm^{-1} excitation to the electronic transition from the ground state to the first excited level of the S_6 symmetry ion. Based on our measurements, we

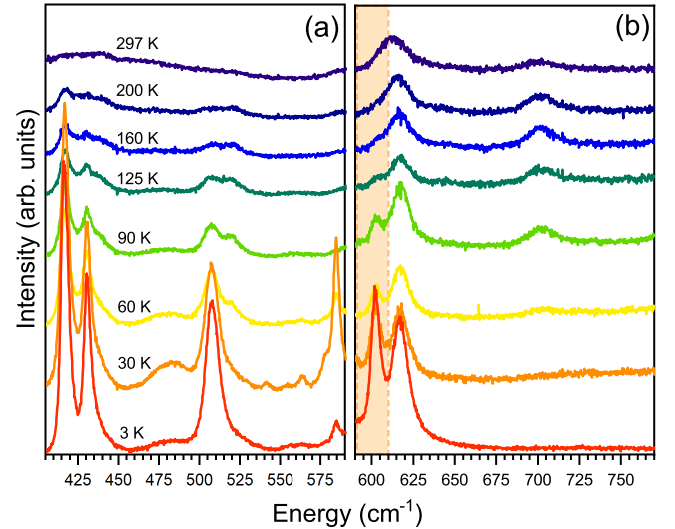


FIG. 8. Temperature dependence of the features having energies greater than 400 cm^{-1} , showing the dramatic evolution of phonons in this region with decreasing temperature. The CEF transition at 602 cm^{-1} is, again, highlighted in orange. Individual spectra have been offset vertically for clarity.

propose a level diagram for the ${}^2F_{7/2}$ manifold of the C_2 and S_6 symmetry ions in Yb_2O_3 , shown in Figure 9. The energies of the CEF excitations measured in this and previous studies, as well as the associated Yb^{3+} ion sites, are summarized in Table II.

Additional supporting evidence for the electronic character of the 336, 376, and 601 cm^{-1} excitations can be found in their magnetic-field dependences. As these levels are Kramers doublets—that is, time-reversal symmetry paired states having opposite angular momentum—a magnetic field is expected to cause these levels to split by an amount that depends linearly on the strength of the magnetic field. As shown in Figure 10 and summarized in Figure 11, we observe that the splitting of Kramers doublets with applied magnetic field is monotonic and gradual. We also observe that both modes that originate from the 376 cm^{-1} transition anomalously increase in energy with increasing field. We will later discuss how the anomalous magnetic field-dependence of the energy and splitting of the 376 cm^{-1} CEF transition may result from coupling to phonon degrees of freedom.

Transitions from the ground states to excited ${}^2F_{7/2}$ states of both the C_2 and S_6 symmetry ions are Raman-allowed by group theory. However, contrary to the reports by Gruber et al. [33], we do not observe any features having an energy of approximately 740 cm^{-1} . Measurements were not performed beyond 955 cm^{-1} in this study, so we are unable to validate the CEF excitation energies from the ground state to the third CEF levels of either the C_2 (1021 cm^{-1}) or S_6 (980 cm^{-1}) ions reported by Gruber et al. [33].

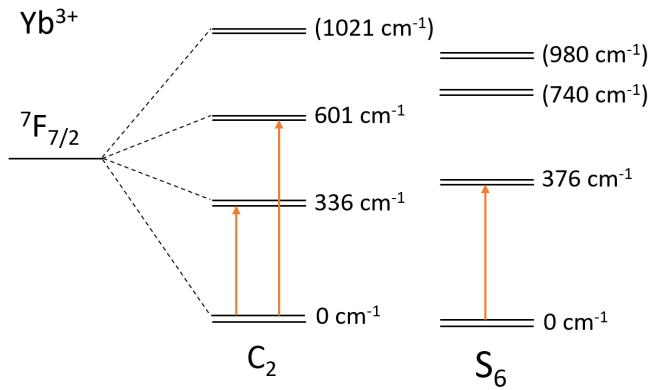


FIG. 9. Proposed low energy CEF level schemes for both Yb^{3+} ion sites in Yb_2O_3 . Arrows depict the observed transitions from the ground state to excited states. Energies presented in parentheses are of levels not observed in this study, but instead are obtained from Ref [33].

3. Temperature- and Field-dependent Anomalies

Our temperature-dependent studies of the Yb_2O_3 spectra reveal three distinct types of anomalies: (i) phonons having energies between $400 - 600 \text{ cm}^{-1}$ with dramatic temperature dependent intensities; (ii) re-entrant electronic excitations that gain and then lose intensity with decreasing temperature; and (iii) soft phonons whose energies decrease with decreasing temperature. Previous Raman scattering reports on Yb_2O_3 have remarked on the weak intensities and broad linewidths of phonons having energies greater than 200 cm^{-1} in spectra obtained at or near room temperature [24, 30–32, 37]. Our results show that these linewidth anomalies persist over a large temperature range between $3 - 300 \text{ K}$.

Further, our results presented in Figure 8 show that above 400 cm^{-1} , only two clear Raman-active features appear in spectra obtained at room temperature. However, as the temperature is lowered, we observe five additional, strong excitations having energies greater than 400 cm^{-1} that emerge and gain intensity. These include five phonons having energies of $415.5, 430.3, 507, 617 \text{ cm}^{-1}$, and one CEF electronic transition having an energy of 602 cm^{-1} , which we discussed in Section III B 2. The assignment of the 602 cm^{-1} mode as a crystal field transition, rather than a phonon mode, is supported by earlier analyses of spectroscopic data by Gruber et al. [33]. Other C-type RESOs feature several Raman-active phonon modes having energies greater than 400 cm^{-1} [24, 30–32, 37], but these phonons do not exhibit dramatic temperature dependences similar to those observed in Yb_2O_3 .

In contrast to the excitations in Yb_2O_3 that gain significant intensity with decreasing temperature, the excitation centered at approximately 702 cm^{-1} loses intensity below 90 K and is ultimately absent in spectra obtained at 30 and 3 K . Several other features gain intensity as the temperature is lowered, before losing intensity as the

temperature is reduced further, beyond 90 K , and are ultimately absent in spectra obtained at 3 K . The most apparent of these re-entrant excitations have energies of $256.3, 294, 347, 584 \text{ cm}^{-1}$. Several other excitations having larger linewidths and weaker, re-entrant intensities are also evident with energies of approximately $481, 520, 541, 563 \text{ cm}^{-1}$. While the temperature dependences of these features suggest that they may be electronic excitations between excited CEF states of the $\text{Yb}^{3+} 7F_{7/2}$ manifolds, we can rule out this interpretation because these features do not have energies coincident with any of the transitions between the $\text{Yb}^{3+} 7F_{7/2}$ levels. We can rule out resonant scattering between excited CEF levels, because of the large Yb_2O_3 bandgap, which is significantly greater than the excitation energy of our laser [38]. Further, we can likely rule out energy transfer reactions, like those we attribute to the anomalous features in Eu_2O_3 , as the re-entrant temperature dependences of these features are inconsistent with the expected temperature dependences for energy transfer reactions [10]. Unfortunately, based on our existing Raman measurements, we are unable to offer a definitive explanation for the anomalous re-entrant temperature dependent behavior of these features, suggesting a potential avenue for future study. Polarization dependent Raman scattering or momentum resolved measurement techniques such as inelastic neutron scattering performed on single crystals may aid in elucidating the origin of these features.

Finally, we observe evidence for strong CEF-phonon coupling in Yb_2O_3 in both our temperature- and magnetic field dependent studies. As shown in Figure 7,

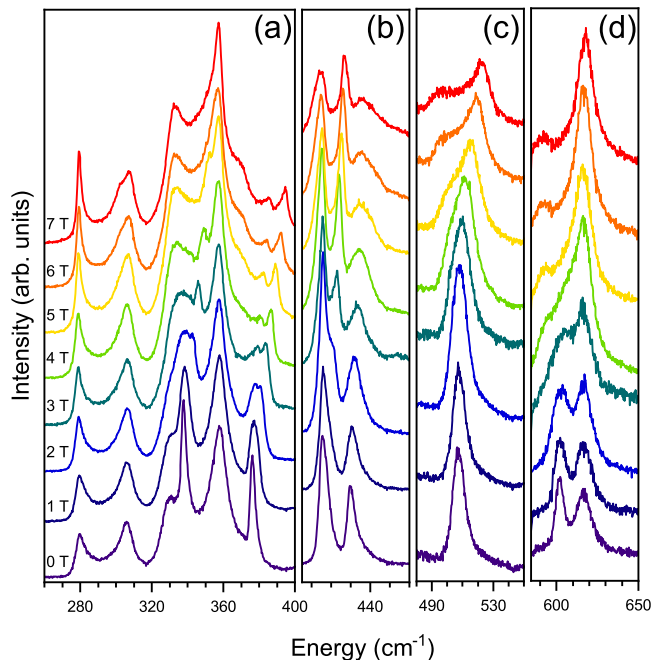


FIG. 10. Magnetic field dependence of the Yb_2O_3 spectra. Individual spectra have been offset vertically for clarity and the vertical scales are different between the subfigures.

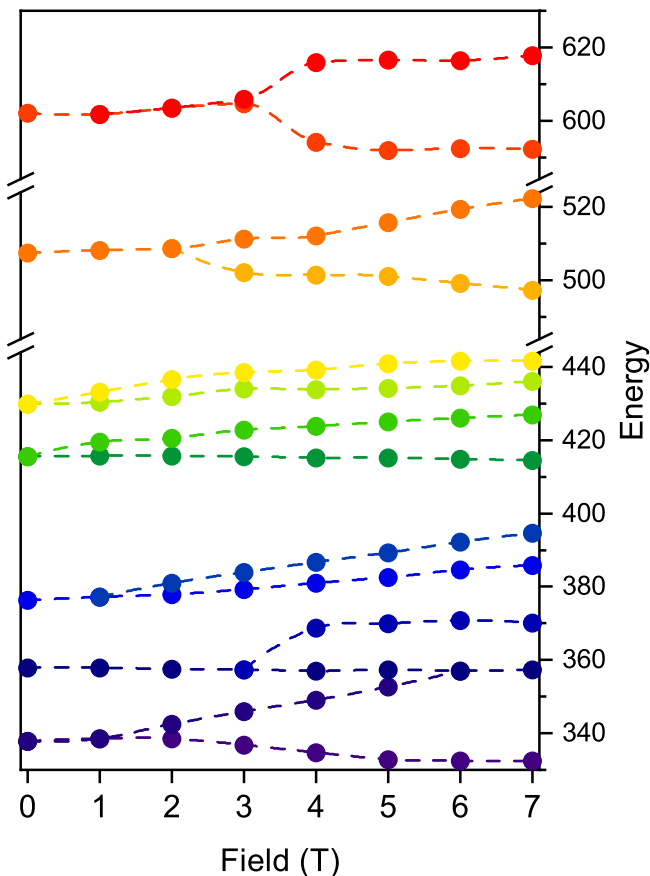


FIG. 11. Summary plot of the magnetic field dependence of the energies of magnetically-active modes in the Yb_2O_3 spectra. Only features which split under an applied magnetic field are included in this summary plot.

four phonons having energies 279.7, 306, 330.8, and 358 cm^{-1} at 3 K anomalously soften by approximately 6 cm^{-1} (2.1%), 3 cm^{-1} (1%), 4.5 cm^{-1} (1.3%), and 6 cm^{-1} (1.6%), respectively, from their room temperature energies as the sample is cooled. Note that heat capacity measurements show no evidence for a structural transition below room temperature under ambient pressure conditions in Yb_2O_3 [33]. Consequently, the phonon softening we observe in this material is not likely associated with structural phase transition.

Similar phonon softening observed in hexagonal, A-type RESOs, Ce_2O_3 [6] and Pr_2O_3 [9] is well explained by the model of vibronic coupling proposed by Thalmeier and Fulde [11]. Thalmeier-Fulde-type coupling between these soft phonons and the nearby CEF excitations in Yb_2O_3 is consistent with both the temperature-dependent softening and the deviation from the trends in phonon energies established by many of the other RESOs [11]. In the Thalmeier-Fulde picture, near-resonance and shared symmetries between phonon and CEF electronic excitations are necessary criteria for vibronic coupling. Given the energetic proximity of the four soft phonons to the 336 and 376 cm^{-1} CEF transitions, the resonance

criterion is well satisfied for these excitations in Yb_2O_3 [11]. Further, all Raman-active phonons have overlapping symmetry with transitions between states of the $J = 7/2$ manifold of the C_2 symmetry Yb^{3+} ions. While we are unable to conclusively identify the symmetries of the ground or excited states of the S_6 symmetry Yb^{3+} ions, the 358 cm^{-1} T_g phonon fulfills the symmetry criterion for all of the allowed transitions between states of the $J = 7/2$ manifold of the S_6 symmetry ions. Therefore, we find that the necessary and sufficient conditions for Thalmeier-Fulde-type vibronic coupling are well satisfied in Yb_2O_3 .

Thalmeier-Fulde-type coupling leads to mixing of the phononic and electronic character of the coupled excitations, renormalizing the bare excitations into hybrid vibronic states. As shown in Figure 10 and summarized in Figure 11, we find additional evidence for hybrid electronic-phononic character of the 357, 415.5, 429, and 507 cm^{-1} modes based on their anomalous magnetic field-dependences. Specifically, as the magnetic field is increased, we observe splitting of these phonons and level-repulsion behavior between these phonons and the nearby CEF electronic excitations as they shift to higher energies. Further, the 306.5 cm^{-1} peak develops an asymmetric lineshape at high fields, while the 279.7 cm^{-1} peak narrows significantly with increasing field.

Splitting of these phonons with external magnetic fields suggests there is coupling between the lattice and some spin- or other angular momentum-degree of freedom in Yb_2O_3 . Given that Yb_2O_3 exists in the paramagnetic phase at $T = 3\text{ K}$ [34], we can rule out coupling to spin-wave excitations. Additionally, we rule out an interpretation involving coupling to spins of conduction electrons because Yb_2O_3 is an insulator. Consequently, the observed splitting of these phonons is most consistent with the hybrid electronic-phononic character of these modes [39, 40], offering additional support that Thalmeier-Fulde-type vibronic coupling significantly impacts the low energy electronic and phonon spectra of Yb_2O_3 .

IV. Summary and Conclusions

In summary, the results presented here allow us to identify specific mechanisms responsible for anomalous phonon behavior in rare-earth sesquioxides and illustrate the varied manifestations of the coupling between phonons and low energy electronic excitations in these materials. Upon comparing the spectra of these two systems, we find that different mechanisms are likely responsible for the observed phonon softening in Yb_2O_3 and Eu_2O_3 . Specifically, we find evidence of strong Thalmeier-Fulde-type CEF-phonon vibronic coupling in Yb_2O_3 based on our observations of temperature-dependent phonon softening, field-dependent splitting of phonons, and avoided-level repulsion behavior between electronic excitations and phonons. In contrast, we find evidence of defect-mediated electron-phonon coupling in Eu_2O_3 , based on the presence of Raman-forbidden,

infrared-active phonons and electronic excitations in our measured spectra. Looking forward, we expect that Yb_2O_3 and Eu_2O_3 are not unique amongst the RESOs in displaying the hallmarks of strong electron-phonon coupling. Many other RESOs display subtle anomalous phonon behavior, reflecting diverse, novel realizations of interactions between the lattice and electrons

associated with the close proximity and shared symmetries of phonons and rare-earth derived CEF electronic excitations prevalent in these materials.

Acknowledgments

Research was supported by the National Science Foundation under Grant No. NSF DMR 1800982 (J.E.S and S.L.C) and DMR-1455264-CAR (A.C. and G.J.M.).

-
- [1] K. I. Kugel' and D. I. Khomskii, Soviet Physics Uspekhi **25**, 231 (1982).
- [2] R. J. Elliott, R. T. Harley, W. Hayes, S. R. P. Smith, and B. Bleaney, Proceedings of the Royal Society of London. A. Mathematical and Physical Sciences **328**, 217 (1972).
- [3] K. Kirschbaum, A. Martin, D. A. Parrish, and A. A. Pinkerton, Journal of Physics: Condensed Matter **11**, 4483 (1999).
- [4] K. Kishimoto, T. Ishikura, H. Nakamura, Y. Wakabayashi, and T. Kimura, Phys. Rev. B **82**, 012103 (2010).
- [5] T. Kolodiaznyy, H. Sakurai, M. Avdeev, T. Charoonsuk, K. V. Lamonova, Y. G. Pashkevich, and B. J. Kennedy, Phys. Rev. B **98**, 054423 (2018).
- [6] A. Sethi, J. E. Slimak, T. Kolodiaznyy, and S. L. Cooper, Phys. Rev. Lett. **122**, 177601 (2019).
- [7] S.-W. Cheong and M. Mostovoy, Nature materials **6**, 13 (2007).
- [8] T. Birol, N. A. Benedek, H. Das, A. L. Wysocki, A. T. Mulder, B. M. Abbett, E. H. Smith, S. Ghosh, and C. J. Fennie, Current Opinion in Solid State and Materials Science **16**, 227 (2012), multiferroics.
- [9] J. E. Slimak, A. Sethi, T. Kolodiaznyy, and S. L. Cooper, Phys. Rev. Res. **2**, 043169 (2020).
- [10] M. Buijs, A. Meyerink, and G. Blasse, Journal of Luminescence **37**, 9 (1987).
- [11] P. Thalmeier, Journal of Physics C: Solid State Physics **17**, 4153 (1984).
- [12] P. Thalmeier and P. Fulde, Phys. Rev. Lett. **49**, 1588 (1982).
- [13] D. T. Adroja, A. del Moral, C. de la Fuente, A. Fraile, E. A. Goremychkin, J. W. Taylor, A. D. Hillier, and F. Fernandez-Alonso, Phys. Rev. Lett. **108**, 216402 (2012).
- [14] M. Ye, X. Xu, X. Wang, J. Kim, S.-W. Cheong, and G. Blumberg, Phys. Rev. B **104**, 085102 (2021).
- [15] J. Gaudet, A. M. Hallas, C. R. C. Buhariwalla, G. Sala, M. B. Stone, M. Tachibana, K. Baroudi, R. J. Cava, and B. D. Gaulin, Phys. Rev. B **98**, 014419 (2018).
- [16] L. Ben Farhat, M. Amami, E. Hlil, and R. Ben Hassen, Materials Chemistry and Physics **123**, 737 (2010).
- [17] E. Staritzky, Analytical Chemistry **28**, 2023 (1956).
- [18] Z. K. Heiba, M. Bakr Mohamed, M. A. Abdelslam, and L. H. Fuess, Crystal Research and Technology **46**, 272 (2011).
- [19] G. J. McCarthy, Journal of Applied Crystallography **4**, 399 (1971).
- [20] B. J. Kennedy and M. Avdeev, Australian Journal of Chemistry **64**, 119 (2011).
- [21] J. Blanus, M. Mitric, D. Rodic, A. Szytula, and M. Slaski, Journal of Magnetism and Magnetic Materials **213**, 75 (2000).
- [22] Z. K. Heiba, Y. Akin, W. Sigmund, and Y. S. Hascicek, Journal of Applied Crystallography **36**, 1411 (2003).
- [23] M. V. Abrashev, N. D. Todorov, and J. Geshev, Journal of Applied Physics **116**, 103508 (2014).
- [24] G. Schaack and J. A. Koningsstein, J. Opt. Soc. Am. **60**, 1110 (1970).
- [25] M. W. Urban and B. C. Cornilsen, Journal of Physics and Chemistry of Solids **48**, 475 (1987).
- [26] J. Łazewski, M. Sternik, P. T. Jochym, J. Kalt, S. Stankov, A. I. Chumakov, J. Göttlicher, R. Rüffer, T. Baumbach, and P. Piekarczyk, Inorganic Chemistry **60**, 9571 (2021), pMID: 34143607.
- [27] R. F. Balabaeva, I. A. Vasileva, I. S. Sukshina, and A. N. Rybnikova, Russian Journal of Physical Chemistry A **70**, 43 (1996).
- [28] Chul Hyun Yo, Seok Keun Ko, Hui Jun Won, and Jae Shi Choi, Journal of Physics and Chemistry of Solids **45**, 899 (1984).
- [29] W. Xie, C. Zou, and D. Bao, physica status solidi (a) **214**, 1600874 (2017).
- [30] N. Dilawar Sharma, J. Singh, A. Vijay, K. Samanta, S. Dogra, and A. K. Bandyopadhyay, The Journal of Physical Chemistry C **120**, 11679 (2016).
- [31] J. Cui and G. A. Hope, Journal of Spectroscopy **2015** (2015).
- [32] S. D. Pandey, K. Samanta, J. Singh, N. D. Sharma, and A. K. Bandyopadhyay, AIP Advances **3**, 122123 (2013).
- [33] J. B. Gruber, R. D. Chirico, and E. F. Westrum, The Journal of Chemical Physics **76**, 4600 (1982).
- [34] D. Rojas, J. Espeso, L. R. Fernandez, and L. F. Barquín, Ceramics International **48**, 879 (2022).
- [35] N. Huang and J. Van Vleck, Journal of Applied Physics **40**, 1144 (1969).
- [36] N. Yamada, S. Shionoya, and T. Kushida, Journal of the Physical Society of Japan **32**, 1577 (1972).
- [37] J. E. Slimak, A. Sethi, A. Cote, G. J. MacDougall, and S. L. Cooper, results of Raman scattering studies of C-type sesquioxides: Gd_2O_3 , Dy_2O_3 , Tb_2O_3 . (unpublished).
- [38] T. Ogawa, S. Kobayashi, M. Wada, C. A. J. Fisher, A. Kuwabara, T. Kato, M. Yoshiya, S. Kitaoka, and H. Moriwake, Phys. Rev. B **93**, 201107 (2016).
- [39] P. Thalmeier and P. Fulde, Zeitschrift für Physik B Condensed Matter **26**, 323 (1977).
- [40] G. Schaack, Solid State Communications **17**, 505 (1975).